LUND UNIVERSITY

MASTERS THESIS

Coulomb drag in parallel nanowires

Author:
David DAI

Supervisor:
Martin LEIJNSE
Martin JOSEFSSON

A thesis submitted in fulfillment of the requirements for the degree of Master of Science in Engineering

in the

Solid State Physics Department

February 17, 2020

LUND UNIVERSITY

Abstract

Faculty of Engineering
Solid State Physics Department

Master of Science in Engineering

Coulomb drag in parallel nanowires

by David DAI

In this project the transport phenomenon Coulomb drag is studied in a 1D system comprised of two nanowires in parallel. Specifically, a driving current across the active wire generated a drag current in the passive wire, and we studied how Coulomb drag influenced both the driving and drag currents.

The theoretical calculations used in this project are based on the approach made by Gurevich et al. [1]. The approach is to solve the Boltzmann transport equation describing the Coulomb drag using an iterative method. What is different in our approach is that we iterated until we found a converged solution unlike Gurevich et al. who only iterated once. We also calculated the change in the driving current due to Coulomb drag which was not made by Gurevich et al..

Our study showed that the drag current is linear as a function of applied bias voltage in both the passive and active wires in the small bias region. A non-linear drag current in the passive wire in the large bias regime where linear response theory no longer holds was also shown in our study. The temperature dependence of the drag and driving currents were also calculated. The results showed that the drag current generated in the passive wire has a linear temperature dependence while the temperature dependence of the current in the active wire was barely affected by the presence of Coulomb drag because the driving current is much larger than the generated drag current. We also found that the drag current has an exponential dependency of inter-wire separation distance, which coincides with the predictions of Gurevich et al. [1]. Lastly, our numerical calculations showed that the number of iterations required to reach a converged solution are few but increases if parameters corresponding to stronger electron-electron interaction are used.

Acknowledgements

First and foremost, I would like to thank my supervisors Martin Leijnse and Martin Josefsson for their patience and support since day one of my masters project. I also want to thank Martin Leijnse for giving me the opportunity to attend to various meetings and listen to talks given by researchers in the FTF department of LTH, and Martin Josefsson for helping me with various questions and problems I have encountered in this project.

I want to thank Gustaf Söderlind for discussions regarding numerical methods.

Contents

Chapter 1

Introduction

The goal of this project is to study how Coulomb drag between two parallel nanowires influences the current in each wire. This is the first step towards studying a thermocouple with interactions.

1.1 Why thermocouple?

A sustainable development is sought in today's development in society, economy and science. In the field of science, this implies e.g. a development of eco-friendly technologies. One such development is to produce cleaner forms of energy in order to curb the greenhouse effect. Thermoelectric (TE) devices are increasingly being seen to have the potential for this purpose. They have the ability to directly convert heat to electric energy, meaning waste heat could in principal be utilized to generate electricity. These devices also have the advantage of not containing any mechanically moving parts which make them robust. But, they have one problem which has prevented them from being widely used, namely low intrinsic efficiency. To achieve high intrisic efficiency, TE devices are required to be made of a material showing high electrical conductance but low thermal conductance. Common bulk materials do not have this property since they obey Wiedemann-Franz law $\kappa/\sigma = L_N T$, where κ is the thermal conductivity, σ is the electric conductivity, L_N is the Lorentz number and T is the temperature [2]. There are however many ongoing researches to find new materials suited for TE devices which yields a better intrinsic efficieny. [3]

A TE device is driven by the thermoelectric effect. It has two main functions, 1) converting waste heat to electricity and 2) converting electricity to thermal energy for heating or cooling. [3] A thermocouple is a type of TE device, see figure 1.1, which consists of a hot and a cold side with two pieces of objects connecting them together. Both objects usually consist of semiconductors, one p-doped and one n-doped. The hot and cold side at the end of the semiconductor produce a temperature gradient/difference over it which in turn produces an electron current and a hole current through the thermoelectric effect. This results in an electric current flowing through the thermocouple as seen in figure 1.1.

Previously, it was mentioned that the efficiency of TE devices needs to be further improved, this also holds for thermocouples. The intrinsic efficiency is $\eta = P_E/Q_{in}$, where P_E is the produced electric power and Q_{in} is the heat per unit time supplied to the device. For a bulk metal, see figure 1.2 (A), we have that electrons can flow from the hot to the cold side and vice versa. Having a flow of electrons means that there is also a heat flow. The intrinsic efficieny would be improved if one could, for example, prevent the flow of low temperature electrons from the cold to the hot side, which can be achieved by replacing the bulk metal with a nanostructure such as nanowire, see figure 1.2 (B). Preventing this flow helps to maintain the temperature difference thus reducing Q_{in}. In general, nanostructures work as energy filters, they

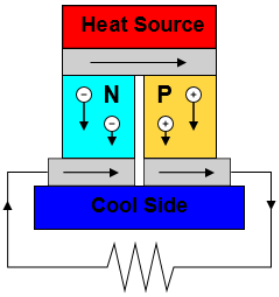

FIGURE 1.1: A thermocouple. Two semiconductors coupled to a heat source and a cold side, one being n-doped (N) and the other being p-doped (P). The arrows in the figure show the direction of the current. Figure taken from [4].

prevent charge carriers of certain energies from being transported through the material due to their transmission function $T(E)$, meaning electrons with energy E such that $T(E) \neq 0$ can flow through the wire. Comparing the metal and the nanowire case (figure 1.2), we see that $T(E)$ has prevented the electron flow at lower energies, and the heat flow at lower energies. This means that, between the metal and nanowire case, the netcurrent is larger and the heat flow is smaller in the nanowire case. This in turn means that η is larger in the nanowire case compared to the metal case.

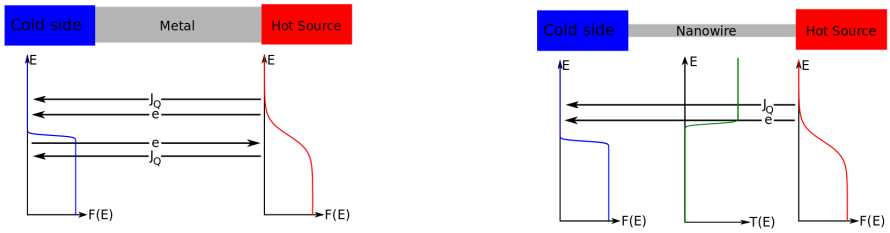

(A) (B)

FIGURE 1.2: Comparison between electron currents in (A) bulkmaterial and (B) nanowire, where we have assumed constant density of states in both materials. In the figures, J_Q stands for heat current, e for electron current, $F(E)$ for Fermi-Dirac distribution and $T(E)$ for transmission function.

By using NWs instead of bulk material, the size of a thermocouple can be made in nanometer size. This means the NWs in the device will be in close proximity and the charge carriers in each wire can, in theory if close enough, interact with each other through Coulomb drag. Coulomb drag is a transport phenomenon where Coulomb interaction between charge carriers belonging to two electrically isolated conductors generates a voltage in one conductor when an electric current is passing through the other. [5] For example, if there are two NWs in parallel, NW1 connected to a ampere meter and NW2 to a battery, then the charge carriers in NW2 will generate a current in NW1 due to Coulomb drag, see figure 1.3. The presence of Coulomb drag between the wires in a thermocouple in the case the separation distance is small is expected, however, how strong influence it has on the thermocouple's performance is not known.

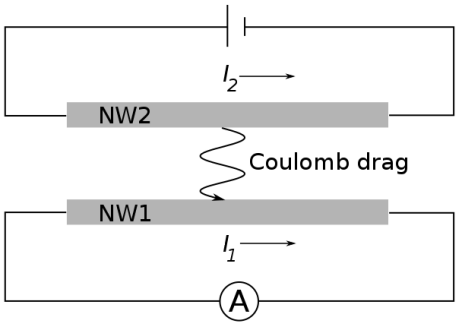

FIGURE 1.3: Coulomb drag between two nanowires.

1.2 Electron transport

1.2.1 Diffusive transport

In the Drude model, the valence electrons of a metal are free in the sense that they are not bound to any atom. The free electrons are assumed to form an ideal classical gas, where classical means the electrons do not obey Pauliprinciple. The electrons can also be accelerated by an external electical field. On average, the electrons will, before scattering, travel the distance λ_{MFP} (called mean free path) during the time τ (called collision time). The scattering can be with e.g. a phonon or an impurity atom. It is assumed that the average velocity of the electron is zero after the scattering, and the electron will accelerate again due to the external field. The overall effect is that the electrons appears to be moving at a constant velocity (called the drift velocity). This type of transport is called diffusive transport, which occurs at high temperatures. The Drude model can also be applied to other materials such as semiconductors. [2]

In the general case, the diffusive transport in a metal and semiconductor is studied by using the integro-differential equation called the Boltzmann transport equation. Its solution is a distribution function which can be used to derive other wanted physical quantities, e.g. current density. A further description of the Boltzmann transport equation and its implementation in this project will be given in section 2.1.

1.2.2 Low temperature physics

The opposite of diffusive transport called ballistic transport, that is the transport of charge carriers without scattering, is more likely to occur as the temperature decreases, since the mean free path which increases as temperature decreases. We have ballistic transport in nanowires if the mean free path is longer than the wire length. [2, 6]

In a truely 1D quantum wire, there would be only one conduction band and valence band. In the case of a quasi-1D wire, such as a nanowire, we instead have several sub-bands. The electrons can transition from one sub-band to another given the thermal energy is greater than the energy gap separating the sub-bands [7]. When the temperature is sufficiently low, such that the corresponding thermal energy is smaller than the energy difference between the first and second sub-bands, we can approximate a nanowire as being one-dimensional because there is only one populated sub-band for sufficiently low electron densities.

1.2.3 Landauer-Büttiker formalism

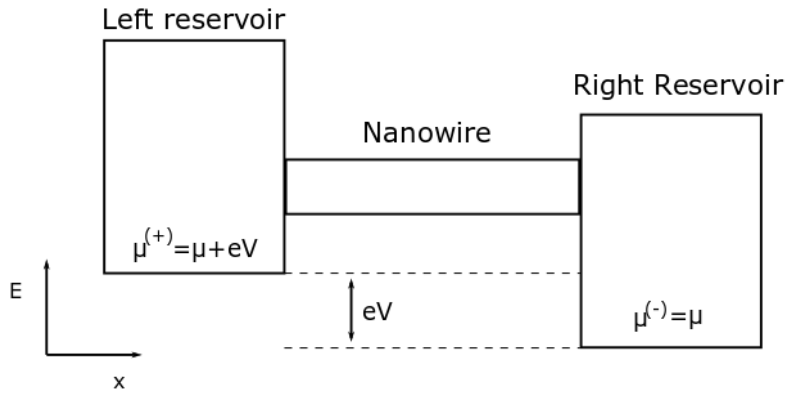

FIGURE 1.4: Schematic of a nanowire connected to two Fermi-liquid reservoirs. The difference in chemical potential is due to an external voltage V applied across the wire. Figure and figure text taken from [8].

For a one-dimensional system or quasi one-dimensional system (such as a nanowire), the conduction of electrons can be calculated using the Landauer-Büttiker formalism [9, 10]. Figure 1.4 shows a schematic picture of the model, a nanowire connected to two Fermi-liquid reservoirs. In this approach, the conduction is viewed as a transmission problem. The current is calculated by considering the contributions from the current going from the left to the right reservoir and from the current in the opposite direction. The current is given by [8]

$$J = \frac{2e}{h} \sum_n \int_{-\infty}^{\infty} T_n(E)[F^{(0)}(E, \mu^{(+)}, n) - F^{(0)}(E, \mu^{(-)}, n)]\, dE, \tag{1.1}$$

where n refers to the transverse quantum number, $T_n(E)$ is the transmission function, $F^{(0)}$ is the Fermi-Dirac distribution, μ is the chemical potential and E is the energy. The electrons going from the left to the right reservoir depends on $\mu^{(+)}$, the chemical potential in the left reservoir. And the left-moving electrons depend on $\mu^{(-)}$, the chemical potential in the right reservoir.

At temperature $T = 0$, the Fermi-Dirac distribution can be rewritten as a step function and the current becomes after carrying out the integration

$$J = \frac{2e^2}{h} V \sum_n T_n(E), \tag{1.2}$$

where V is the applied voltage across the wire.

In the Landauer-Büttiker formalism, fully ballistic transport means the transmission of charge carriers is unhindered in the wire, that is the transmission function $T_n(E)$ is 1. The ballistic current at $T = 0$ is then

$$J_{ball} = \frac{2NVe^2}{h}, \tag{1.3}$$

where N is the total number of occupied one-dimensional channels.

1.3 Coulomb drag

As already described in section 1.1, Coulomb drag is a transport phenomenon where Coulomb interaction between charge carriers belonging to two electrically isolated conductors generates a voltage in one conductor when an electric current is passing through the other. [5]

The existence of Coulomb drag was first suggested by Pogrebinski [11]. Since then, studies of Coulomb drag in two-dimensional systems have been conducted extensively [12]. In contrast, there are less studies of Coulomb drag in one-dimensional systems, in particular experimental studies.

For one-dimensional systems, there are two approaches describing Coulomb drag. The historically first approach is based on a Fermi liquid model done by Gurevich *et al.* [1], which will be further described in section 2.2. The second approach is within the framework of a Luttinger liquid, and will not be covered.

1.3.1 Limitation of Fermi liquid model of 1D Coulomb drag and Luttinger liquid model

The use of a Luttinger liquid approach to explain Coulomb drag arose from the limitations of describing a fermionic one-dimensional system using the Fermi liquid model. Luttinger liquid is a theoretical model describing interacting fermions in a 1D conductor (such as a quantum wire), which differs from the Fermi liquid that neglects interactions between fermions [13]. In 2D and above, the electrons can move through space without necessarily encountering each other at low electronconcentrations, which is not true for the 1D case. In a one-dimensional system, electrons will collide with one another as they move towards one direction or the other. [8] For example, a fast moving electron will collide with a slower moving electron in front of it assuming both electrons travel in the same direction. Thus, the mean-field quasi particle formalism used to describe Fermi liquids can no longer be applied because only collective motion can occur. Also, perturbation theory cannot be used to determine the effect of interactions in one dimensional Fermi liquid model. [8]

However, both the Luttinger liquid and the Fermi liquid aproaches give the same predictions in some cases, e.g. the maximum drag resistance R_D decays exponentially with increasing inter-wire separation. The main difference between the two models is shown in the temperature dependence of the drag effect. The temperature dependence is linear in the Fermi liquid model while the Luttinger liquid model predicts a varied dependence of temperature depending on the relative magnitudes of the length scales and energy of the systems. For example, Luttinger liquid predicts a power-law dependence on temperature $R_D \propto T^x$, where x is determined by the Luttinger liquid parameters. [14]

1.3.2 Experimental Coulomb drag results for one-dimensional systems

Experiments of one-dimensional Coulomb drag between quantum wires coupled at nanoscale has been made by Laroche [8]. It was found that the temperature dependence of the drag resistance was consistent with expectations from the Luttinger liquid description of Coulomb drag. Experimental findings of Coulomb drag in another one-dimensional system of Debray *et al.* [15] could also use the Luttinger liquid model to explain the temperature dependence found from their measurements.

Another experimental study performed by Yamamoto et al. [16] found negative Coulomb drag for parallel coupled quantum wires, in which electrons flow in the

opposite directions between the wires. This only occurred under the conditions of low density, high magnetic field, and low temperature. The results could not be explained by the Fermi liquid approach to Coulomb drag, and they proposed a Coulomb drag model in which formation of a Wigner crystal state in the drag wire and a particle-like state in the drive wire was taken into account.

Chapter 2

Theory

2.1 Boltzmann Transport Equation

The equilibrium distribution of an electron gas in a NW is the Fermi-Dirac function,

$$F^{(0)}(E,\mu) = \frac{1}{1+\mathrm{e}^{(E-\mu)/k_BT}}, \tag{2.1}$$

where $E(\mathbf{r},\mathbf{p})$ is the total energy of an electron, μ the chemical potential, k_B the Boltzmann constant and T the temperature. In the case the electron gas is out of equilibrium we can solve the Boltzmann transport equation (BTE) [3] to obtain the distribution function. The BTE in one dimension is

$$\frac{\partial F}{\partial t} + v\frac{\partial F}{\partial x} + f\frac{\partial F}{\partial p} = \left.\frac{\partial F}{\partial t}\right|_{coll} + s(x,p,t), \tag{2.2}$$

where $F = F(x,p,t)$ is the (unknown) distribution function, t is the time, v is the velocity of the electron, x is the position, f is the force acting on the electrons, p is the momentum of electrons, $\left.\frac{\partial F}{\partial t}\right|_{coll}$ (called collision integral) describes the interactions between electrons and $s(x,p,t)$ describes the carrier generation and recombination processes (photogeneration or recombination through defects). [3]

Due to Heisenberg's uncertainty principal, a quantum state cannot be labeled by both p and x, but this is assumed to be possible in the Boltzmann transport equation because it is a semi-classical approach.

Finding the distribution function of a given system is of great interest because it can be used to obtain various quantities of interest such as the carrier and current densities. In our case, we are interested in finding the current, which is given by

$$\begin{aligned} J(x,t) &= e\sum_{p=-\infty}^{\infty} v(p)F(x,p,t) \\ &= e\sum_{p=0}^{\infty}[v(p)F^{(+)}(x,p,t) - v(-p)F^{(-)}(x,p,t)] \\ &= \frac{eL}{2\pi\hbar}\int_0^{\infty} dp\ [v(p)F^{(+)}(x,p,t) - v(-p)F^{(-)}(x,p,t)], \end{aligned} \tag{2.3}$$

where the distribution function has been decomposed into distribution functions of right moving electrons $F^{(+)}(x,p,t)$ and left moving electrons $F^{(-)}(x,p,t)$ and the current is given by their difference in the second equality. The continuum limit has been used in the third equality.

2.2 Review of Coulomb drag in two quantum wires

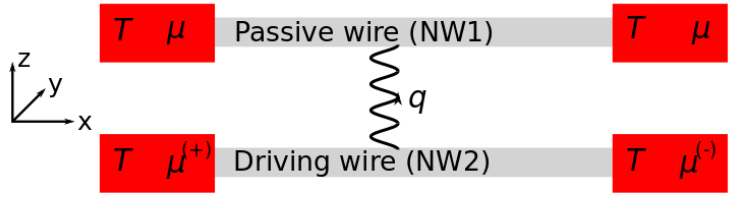

FIGURE 2.1: Schematic picture of Gurevich's model.

In this section, we are presenting previous work made by Gurevich et al. [1]. They calculate the Coulomb drag between two parallel, ballistic quantum wires using the BTE. In their model, see figure 2.1, the BTE of the passive wire was reduced to

$$v(p_1)\frac{\partial F_1(x_1,p_1,n_1)}{\partial x_1} = \left.\frac{\partial F}{\partial t}\right|_{coll}, \tag{2.4}$$

by studying the system in a stationary state ($\frac{\partial F}{\partial t} = 0$), with ballistic electrons ($f = 0$) and without the presence of carrier generation and recombination processes ($s(x,p,t) = 0$). Since the system is comprised of two quantum wires, we have introduced subscripts 1 and 2 to distinguish the variables belonging to the passive and driving wire, respectively. Each wire has several sub-bands, which are denoted by n_i for wire i. Also, electron tunneling between the wires is not included in the model by assuming that the wires are separated too far for tunneling but close enough for Coulomb interactions. Assuming the resulting drag current in the passive wire due to Coulomb drag will be much smaller than the driving current in the driving wire means the bac kaction of the driving wire and the BTE for the driving wire can be neglected.

The collision integral is

$$\left.\frac{\partial F}{\partial t}\right|_{coll} = 2\sum_{p_2}\sum_{q}\sum_{n_2} w(1,p_1+q,n_1;2,p_2-q,n_2 \leftarrow 1,p_1,n_1;2,p_2,n_2)\mathcal{P}, \tag{2.5}$$

with

$$\begin{aligned}\mathcal{P} =& F_1(x_1,p_1+q,n_1)F_2(x_2,p_2-q,n_2)[1-F_1(x_1,p_1,n_1)][1-F_2(x_2,p_2,n_2)] \\ &- F_1(x_1,p_1,n_1)F_2(x_2,p_2,n_2)[1-F_1(x_1,p_1+q,n_1)][1-F_2(x_2,p_2-q,n_2)].\end{aligned} \tag{2.6}$$

The first and second term of eq (2.6) corresponds to the gain and loss of electrons in $F_1(x_1,p_1,n_1)$, respectively. Knowing that $F(x,p,n)$ is the probability of an electron occupying the state described by (x,p,n) and $[1-F(x,p,n)]$ is the probability of (x,p,n) being unoccupied, we see that the gain term describes an electron from $F_1(x_1,p_1+q,n_1)$ that scatters with an electron from $F_2(x_2,p_2-q,n_2)$ such that the electrons end up in empty states described by $[1-F_1(x_1,p_1,n_1)]$ and $[1-F_2(x_2,p_2,n_2)]$ after the scattering. Similar reasoning holds for the loss term.

The scattering probability, w in eq (2.5), can be determined by using Fermi's golden rule (assuming the scattering can be described by perturbation theory)

$$w = \frac{2\pi}{\hbar}|\langle 1, p_1+q; 2, p_2-q|V_{ee}|1, p_1; 2, p_2\rangle|^2 \times \delta(E_1(p_1,n_1)+E_2(p_2,n_2)-E_1(p_1+q,n_1)+E_2(p_2-q,n_2)), \quad (2.7)$$

where $V_{ee} = e^2/(4\pi\varepsilon_r\varepsilon_0|x_1-x_2|)$ is the Coulomb interaction between electrons in wire 1 and 2, $E_i(p_i,n_i)$ is the total energy of an electron. The second term (selection rule) is a Dirac delta function, and the argument describes the conservations of energy and momentum during scattering. The energy conservation can be rewritten as

$$E_1(p_1,n_1)+E_2(p_2,n_2)-E_1(p_1+q,n_1)+E_2(p_2-q,n_2) = -\frac{q}{m}(p_1-p_2+q) \quad (2.8)$$

which inserted in the δ-function gives

$$\delta(E_1(p_1,n_1)+E_2(p_2,n_2)-E_1(p_1+q,n_1)+E_2(p_2-q,n_2)) = \frac{m}{|q|}\delta(p_1-p_2+q), \quad (2.9)$$

where m is the electron effective mass. The matrix element of electron-electron interaction can be transformed to

$$\begin{aligned}\langle 1, p_1+q; 2, p_2-q|V_{ee}|1, p_1; 2, p_2\rangle &= \int d^3r_1 \int d^3r_2\ \phi^*(\mathbf{r_1}, n_1)\phi^*(\mathbf{r_2}, n_2) \\ &\quad V(\mathbf{r_1}-\mathbf{r_2})\phi(\mathbf{r_1}, n_1)\phi(\mathbf{r_2}, n_2) \\ &= \frac{1}{L^2}\int d^2r_1^\perp \int d^2r_2^\perp\ \phi^*(\mathbf{r_1^\perp}, n_1)\phi^*(\mathbf{r_2^\perp}, n_2) \\ &\quad V_q(r_1^\perp - r_2^\perp)\phi(\mathbf{r_1^\perp}, n_1)\phi(\mathbf{r_2^\perp}, n_2),\end{aligned} \quad (2.10)$$

where $V_q = \int dx\ V(x, r^\perp)\exp(-iqx)$, $r^\perp = (y,z)$. We have

$$\int_0^L dx_1 \int_0^L dx_2\ V(x_2-x_1)\exp\left(i\frac{q(x_2-x_1)}{\hbar}\right) = \frac{2e^2L}{4\pi\varepsilon_r\varepsilon_0}K_0\left(\frac{|q|d}{\hbar}\right), \quad (2.11)$$

where K_0 is the modified Bessel function of second kind, the wave function in the wires in the x-directions is $\phi(x) = \frac{1}{\sqrt{L}}\exp(ikx)$ with wire-length L and wavenumber k, and d is the separation distance between the two wires. No assumptions are made of what the wave functions are in the yz-plane.

$K_0(\xi)$ can be approximated by an exponential function as [15],

$$K_0(\xi) = \sqrt{\pi/2}e^{-\xi}, \quad \xi \gg 1, \quad (2.12)$$

which that means K_0 behaves exponentially as long as $|q|\,d/\hbar \gg 1$. This approximation will not be used in our calculations but it will be used to explain our obtained results of the relation between drag current and inter-wire separation distance.

The BTE is solved by one iteration. In this approximation the distribution functions in $\mathcal{P}$ are chosen to be the Fermi-Dirac functions,

$$F_i(x_i,p_i,n_i) = F_i^{(0)}(p_i,\mu_i,n_i). \quad (2.13)$$

Using the Landauer-Büttiker approach [1], each wire-end is connected to a separate reservoir, each of them being in equilibrium independently. An electric potential

V applied to the driving wire gives an unequal chemical potential in the right and left reservoirs, $\left|\mu^{(+)} - \mu^{(-)} = eV\right|$. There are both left and right moving electrons in each quantum wire and we can therefore separate the whole distribution function of a wire into $F_i^{(+)} = F_i(x_i, p_i, n_i)$ and $F_i^{(-)} = F_i(x_i, -p_i, n_i)$, which are the distribution functions of right and left moving electrons, respectively. The electrons moving right depend on the chemical potential of the left reservoir ($\mu^{(+)}$) and likewise the left moving electrons depend on the right chemical potential $\mu^{(-)}$. This gives that the distribution term in the collision integral is

$$\begin{aligned}\mathcal{P} =& F_1^{(0)}(p_1+q,\mu,n_1)F_2^{(0)}(p_2-q,\mu^{(-)},n_2)[1-F_1^{(0)}(p_1,\mu,n_1)][1-F_2^{(0)}(p_2,\mu^{(+)},n_2)] \\ &- F_1^{(0)}(p_1,\mu,n_1)F_2^{(0)}(p_2,\mu^{(+)},n_2)[1-F_1^{(0)}(p_1+q,\mu,n_1)][1-F_2^{(0)}(p_2-q,\mu^{(-)},n_2)],\end{aligned} \tag{2.14}$$

where the chemical potential in the passive wire is the equilibrium chemical potential μ since there is no bias voltage applied across that wire. Note that when approximating the distribution functions in $\mathcal{P}$ by Fermi-Dirac functions the collision integral no longer depends on x_1 and x_2, and the analytical solution of the reduced BTE (eq (2.4)) becomes

$$\begin{aligned}F_1^{(+)}(x_1,p_1,n_1) &= \frac{1}{v(p_1)}\frac{\partial F}{\partial t}\bigg|_{coll} x_1 + F_1^{(0)}(E_1,\mu,n_1), \quad p_1>0, \\ F_1^{(-)}(x_1,p_1,n_1) &= \frac{1}{v(p_1)}\frac{\partial F}{\partial t}\bigg|_{coll} (x_1-L) + F_1^{(0)}(E_1,\mu,n_1), \quad p_1<0\end{aligned} \tag{2.15}$$

where the following boundary conditions have been used

$$F_1^{(+)}(0,p_1,n_1) = F_1^{(-)}(L,p_1,n_1) = F_1^{(0)}(E_1,\mu,n_1). \tag{2.16}$$

The drag current in the passive wire is

$$\begin{aligned}J_1 &= e\sum_{n_1}\sum_{p_1=0}^{\infty}[v(p_1)F_1^{(+)}(x_1,p_1,n_1) + v(-p_1)F_1^{(-)}(x_1,-p_1,n_1)] \\ &= e\sum_{n_1}\sum_{p_1=0}^{\infty}\frac{\partial F}{\partial t}\bigg|_{coll} \\ &= e\sum_{n_1}\int_0^{\infty}dp_1\,\frac{L}{2\pi\hbar}\frac{\partial F}{\partial t}\bigg|_{coll},\end{aligned} \tag{2.17}$$

where

$$\begin{aligned}\frac{\partial F}{\partial t}\bigg|_{coll} = 2\sum_{n_2}\int dp_2\,\frac{L}{2\pi\hbar}\int dq\,\frac{L}{2\pi\hbar}\frac{2\pi}{\hbar}|g(q,n_1,n_2)|^2 \\ \times\frac{m}{|q|}\delta(p_1-p_2+q),\end{aligned} \tag{2.18}$$

and

$$g(q,n_1,n_2) = \frac{2e^2}{4\pi\varepsilon_r\varepsilon_0 L}\int d^2r_1^{\perp}\int d^2r_2^{\perp}\left|\phi(\mathbf{r_1^{\perp}},n_1)\right|^2\left|\phi(\mathbf{r_2^{\perp}},n_2)\right|^2 K_0\left(\frac{|q|d}{\hbar}\right). \tag{2.19}$$

The integration limit over the p_1-, p_2- and q-integral in eqs. (2.17) and (2.18) are given

by the scattering mechanism. Only backscattering can occur, because if the initial quasimomentum p_2 before interactions and the final quasimomentum $p_2 - q$ after interactions are of the same sign then $\mathcal{P}$ in the collision integral (2.6) can be shown to be equal to zero. Backscattering and conservation of momentum ($p_1 = p_2 - q$) together yields the following two integration limits

- if $p_1, p_2 \geq 0$ then we must have $q \geq p_2$ so that conservation of momentum $0 \leq p_1 = p_2 - q$ holds. This gives the integrals, sloppily written, $\int_0^\infty dp_1 \int_0^\infty dp_2 \int_{p_2}^\infty dq$.
- if $p_1 \geq 0$, $p_2 \leq 0$ then we must have $q \leq -p_2$ so that conservation of momentum $0 \leq p_1 = p_2 - q$ holds. This gives the integrals, sloppily written, $\int_0^\infty dp_1 \int_{-\infty}^0 dp_2 \int_{-\infty}^{-p_2} dq$.

Eliminating the q-integral by using the Dirac-delta in eq. (2.18), we find

$$J_1 = \frac{me^5 L}{8\pi^4\hbar^4\varepsilon_r^2\varepsilon_0^2} \sum_{n_1,n_2} \int_0^\infty dp_1 \int_0^\infty dp_2 \frac{|g(p_1+p_2, n_1, n_2)|^2}{p_1+p_2} \times F_1^{(0)}(p_1, \mu, n_1)[1 - F_1^{(0)}(p_2, \mu, n_1)] F_2^{(0)}(p_2, \mu^{(+)}, n_2)[1 - F_2^{(0)}(p_1, \mu^{(-)}, n_2)]. \tag{2.20}$$

Further approximations are made by Gurevich et al. [1] to find a more simple expression for J_1 but we do not include them because they will not be used in our model.

2.3 Our model

Our model is based on Gurevich's model with some minor changes. We assume the wires to be purely 1D which means the wave functions in $y-$ and $z-$directions can be dropped from eq (2.10) and $n_1 = n_2 = 1$ in all equations and the summation over sub-bands (n_1 and n_2) can be removed in the collision integral. We also consider the back action of the passive wire to the driving wire, since the produced drag current in the passive wire should also influence the driving wire with Coulomb drag.

Unlike in Gurevich's model, we also want to find the current in our driving wire, hence we need a second BTE. Following the same procedure as in the previous section, we find that the second BTE is

$$v_{n_2}(p_2) \frac{\partial F_2(x_2, p_2)}{\partial x_2} = -\left.\frac{\partial F}{\partial t}\right|_{coll}, \tag{2.21}$$

where the difference is the minus sign in front the collision integral (apart from different x and p). The minus sign appears due to conservation of momentum during electron-electron scatterings in our model. The collision integral can be interpreted as the net momentum gain, and the conservation of momentum then gives us that the net gain in NW1 should give an equal magnitude of net loss in NW2. It can also be derived by following the same procedure as in the previous section. The force f is still set to 0 in wire 2, despite having a bias voltage across it. If this is not the case, then one finds that the electron transport within the wire is no longer ballistic in the absence of wire 1 which contradicts our assumption.

Thus, the coupled BTE in our model are

$$\begin{aligned}
v(p_1)\frac{\partial F_1^{(+)}(x_1,p_1)}{\partial x_1} &= \left.\frac{\partial F}{\partial t}\right|_{coll}, \quad F_1^{(+)}(0,p_1) = F_1^{(0)}(E(p_1),\mu),\\
v(-p_1)\frac{\partial F_1^{(-)}(x_1,-p_1)}{\partial x_1} &= -\left.\frac{\partial F}{\partial t}\right|_{coll}, \quad F_1^{(-)}(L,-p_1) = F_1^{(0)}(E(p_1),\mu),\\
v(p_2)\frac{\partial F_2^{(+)}(x_2,p_2)}{\partial x_2} &= -\left.\frac{\partial F}{\partial t}\right|_{coll}, \quad F_2^{(+)}(0,p_2) = F_2^{(0)}(E(p_2),\mu^{(+)}),\\
v(-p_2)\frac{\partial F_2^{(-)}(x_2,-p_2)}{\partial x_2} &= \left.\frac{\partial F}{\partial t}\right|_{coll}, \quad F_2^{(-)}(L,-p_2) = F_2^{(0)}(E(p_2),\mu^{(-)}),
\end{aligned} \tag{2.22}$$

where we have written a system of four BTEs by distinguishing distribution functions for right and left moving electrons in each wire due to different boundary conditions of each wire end. The energy is $E(p_i) = p_i^2/(2m)$ for $i = 1,2$ where we have set the zero energy level as the bottom of the conduction band. The collision integral, after using our added approximations, is

$$\left.\frac{\partial F}{\partial t}\right|_{coll} = \frac{me^4}{4\pi^3\hbar^3\varepsilon_r^2\varepsilon_0^2}\int_0^\infty dp_{1,2}\,\frac{|K_0(d|p_1+p_2|/\hbar)|^2}{|p_1+p_2|}\mathcal{P}, \tag{2.23}$$

where

$$\mathcal{P} = F_1^{(-)}F_2^{(+)}[1-F_1^{(+)}][1-F_2^{(-)}] - F_1^{(+)}F_2^{(-)}[1-F_1^{(-)}][1-F_2^{(+)}]. \tag{2.24}$$

In the integral, $dp_{1,2}$ means the integral is over dp_2 for wire 1 and dp_1 for wire 2.

We iterate the four BTEs more than once. In the first iteration of NW1 BTEs, we still use the initial guess that the distribution functions are the Fermi-Dirac functions. After the iterations of NW1 ($F_1^{(+)}$ and $F_1^{(-)}$) we update the distribution functions of NW1 in the collision integrals of NW2 to the newly obtained ones. Then, solving the BTEs for NW2 gives us a new pair of distribution functions of NW1 which we substitute in the BTEs of NW1. This cycle then repeats until we reach four converged distribution functions.

The BTE is an integro-differential equation where both the integration operator and differential operator act on the unknown function. We solved each BTE in eq (2.22) by solving the integral part and differential part separately. We first evaluated the collision integral (2.23) using Bode's rule, and then solved the differential part using Euler's method. Due to the singularity at $p_1 + p_2 = 0$ in (2.23) we chose to cut off the singularity by letting $p_{min,\alpha} = 0.2\sqrt{2\mu m}$ for $\alpha = 1,2$, where m is the electron mass. Cut-off at p_{min} will not significantly impact the results at low temperatures where the occupancies of states around p_{min} is almost one in both wires, electrons at such states will not interact with other electrons through Coulomb drag. It will be shown in section 3.1 that the deviation between the solution of BTE with the Fermi-Dirac distribution is around μ.

To calculate the current in wire α from the distribution functions we use

$$J_\alpha(x) = \frac{\int_0^\infty dp_\alpha\, v(p_\alpha)[F_\alpha^{(+)} - F_\alpha^{(-)}]}{\int_0^\infty dp_2\,[v(p_2)F_2^{(0)}(p_2,\mu^{(+)},T) + v(-p_2)F_2^{(0)}(-p_2,\mu^{(-)},T)]}. \tag{2.25}$$

Chapter 3

Results & Discussion

The parameters used in numerical calculations are shown in table 3.1. These values have been applied to all calculations unless other values are specified. Also, we have set effective mass $m_{eff} = 0.26$ and relative permittivity $\varepsilon_r = 11$, which are the values for silicon. The choice of for these values are for the purpose to yield good results for the numerical calculations, and to have somewhat realistic values on certain parameters, such as nanowire length L.

	T [K]	U [V]	μ [eV]	L [nm]
NW1	1	0	$8.6\dot{1}0^{-4}$	1000
NW2	1	$8.6\dot{1}0^{-6}$	$8.6\dot{1}0^{-4}$	1000
	d [nm]			
	20			

TABLE 3.1: Parameters used in numerical calculations.

3.1 Distribution functions

We begin by looking at the solutions of the BTE, that is the distribution functions, which are presented in figure 3.1. We see that all solutions look similar to Fermi-Dirac distributions without any obvious deviations. However, the difference can be clearly seen after subtracting away the corresponding Fermi-Dirac distribution from each solution, see figure 3.2. The corresponding Fermi-Dirac distribution refers to the initial (before iterations) distribution of each wire, hence the 0 in the superscript. Note that in wire 2, the Fermi-Dirac distributions for positive and negative p are not equal because they depend on different chemical potentials, see figure 2.1. We see that the change in each distribution function from its initial Fermi-Dirac distribution is small ($\sim 10^{-6}$). Also, most of the changes happen at around $p = \left|8 \times 10^{-27}\right|$ kgm/s, which coincides with the chemical potential ($\mu \approx 8 \times 10^{-4}$ eV). This means that most of the changes occur close to the chemical potential, which is makes sense due to the small applied bias. The change to each distribution function is only an increase or a decrease within a wire, which corresponds to a gain or a loss of electrons in one direction, respectively. However, the number of electrons in each wire does not change. From figure 3.2, we see an increase in $F_1^{(+)}$ and $F_2^{(-)}$, and a decrease in $F_1^{(-)}$ and $F_2^{(+)}$. Due to the same sign of $F_1^{(+)} - F_1^{(-)}$ and $F_2^{(+)} - F_2^{(-)}$, as seen in figure 3.3, the generated current in NW1 has the same direction as the driving current. These two results make sense because in our model, see figure 2.1, where we have applied a positive bias voltage in the right reservoir of NW2, meaning we have a net flow of electrons from left to right (positive direction) in NW2 and, hence, there should be more electrons flowing in the positive direction in NW1 (increase in

$F_1^{(+)}$) since the scattering probability w is equal in both directions. The decrease in $F_1^{(-)}$ is followed by the increase in $F_1^{(+)}$, the gained electrons in $F_1^{(+)}$ are the backscattered electrons in $F_1^{(-)}$. Since backscattering is the only scattering mechanism in our model, an electron moving in the negative direction in NW1 only scatters with an electron moving in the positive direction in NW2. After the collision, both electrons move in the opposite direction — there is a gain in electrons in $F_1^{(+)}$ and $F_2^{(-)}$, and a decrease in $F_1^{(-)}$ and $F_2^{(+)}$ due to charge conservation. So looking at the increases and decreases in the distribution functions, we can also conclude that the electron flow in NW1, induced by Coulomb drag, will be in the positive direction and the electron current in NW2 will be decreased.

Lastly, we find that charge conservation holds, as it should, which is shown in figure 3.3. By taking the difference of the distribution functions corresponding to electrons moving in the positive and negative directions and finding that the difference is constant in x implies that the current is constant in x, according to eq (2.17). This in turn implies charge conservation.

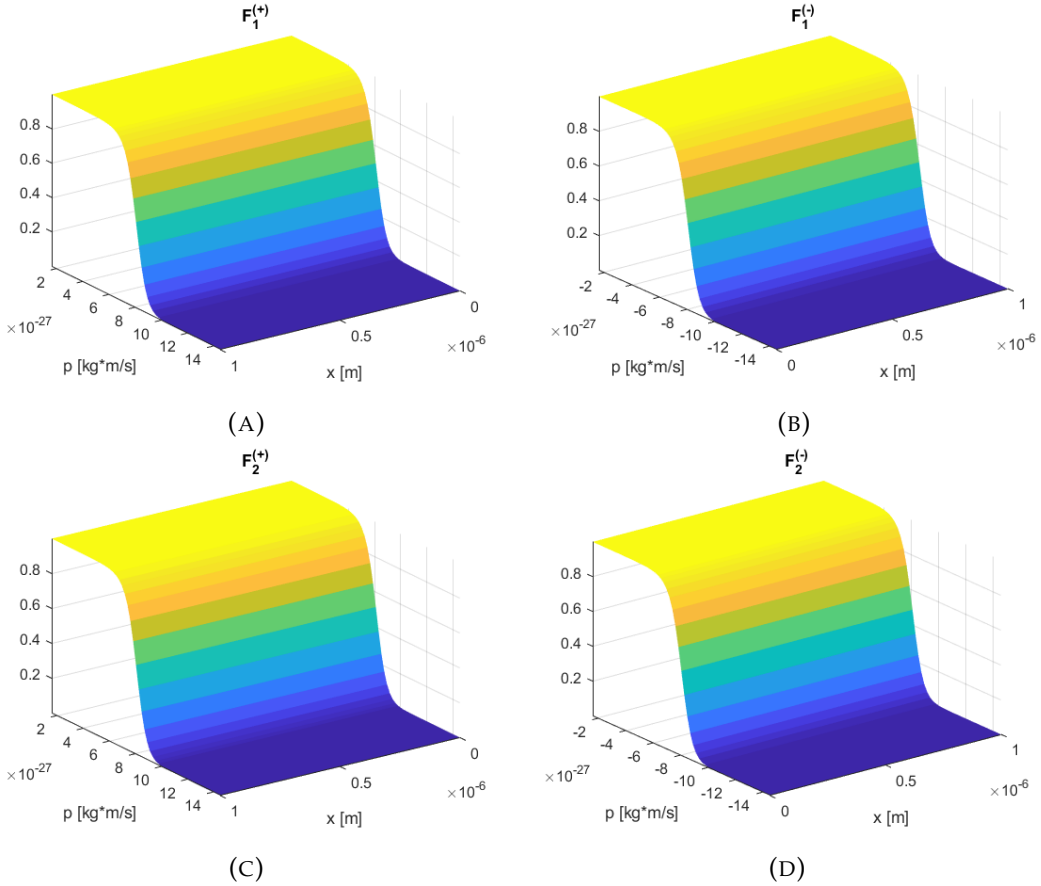

FIGURE 3.1: Solutions of BTE. (A) and (B) are the solutions in NW1 for $p > 0$ and $p < 0$, respectively. (C) and (D) are the solutions in NW2, similar as (A) and (B).

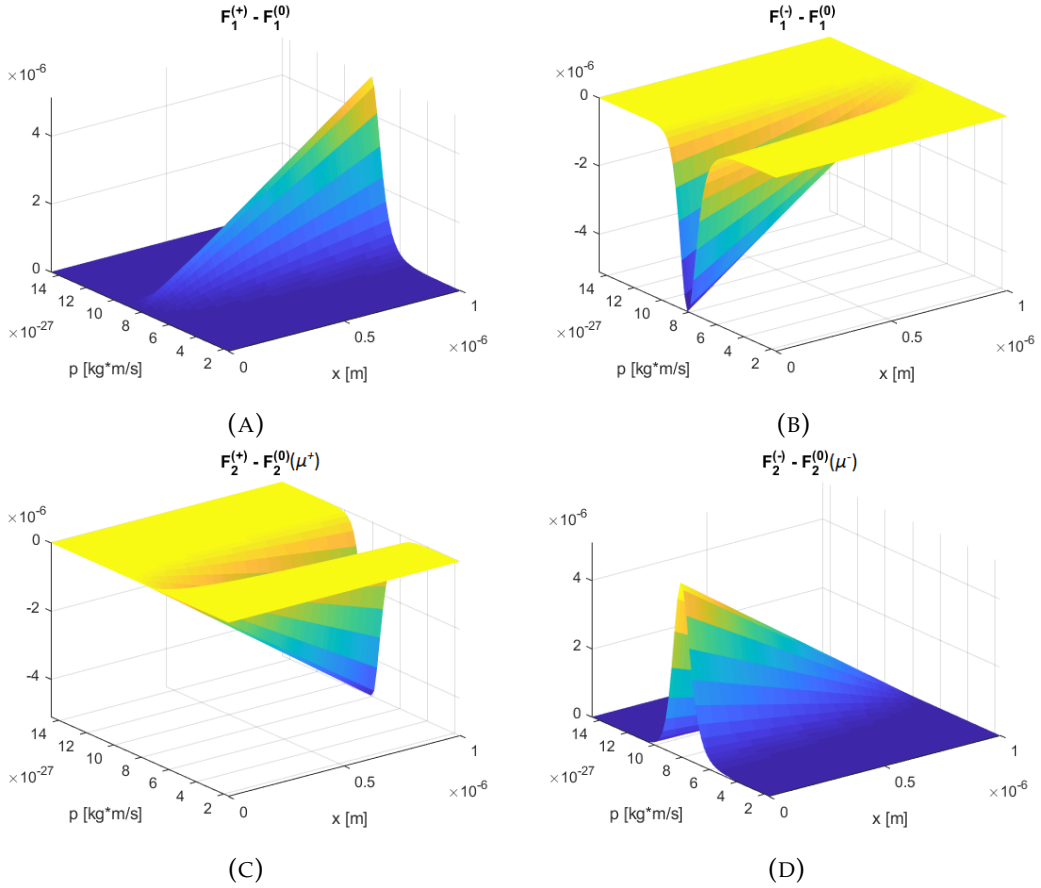

FIGURE 3.2: Changes in distribution functions.

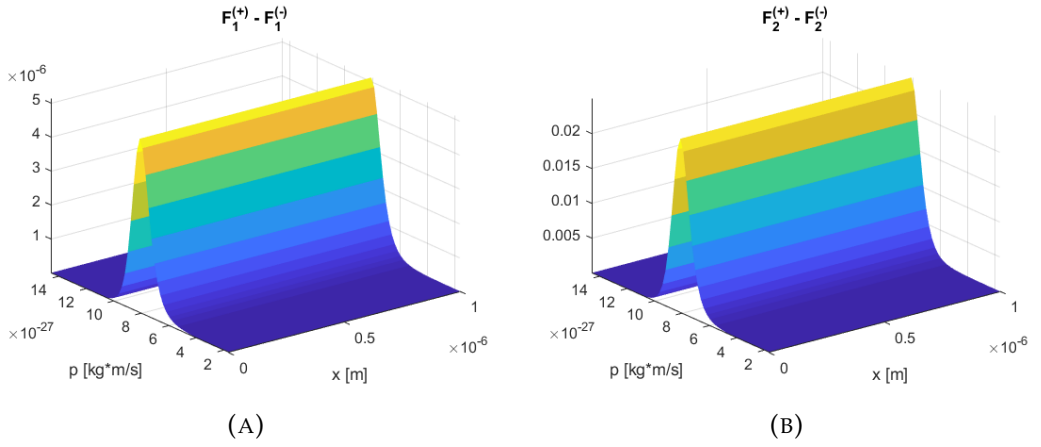

FIGURE 3.3: The difference of left and right distribution functions of each wire. Both (A) and (B) are constant in x which shows that the charge conservation holds.

3.2 Number of iterations

Here we show the number of iterations required for a converged solution to the BTE (distribution function). We use the current to determine the convergence because if the solution has converged after n iterations then the current should remain unchanged for solutions obtained by $m > n$ iterations. The results are presented in

figure 3.4, where we have used the parameters in table 3.1. From the figure we see that only a few iterations are required to reach a converged solution. There is a big jump between the first and second iteration, in comparison to the third and fourth iteration, which shows that doing more than one iteration when solving BTE makes sense.

The number of iterations required depends slightly on the parameters used, see figure 3.5. Parameters giving stronger interactions between the wires require more iterations to reach convergence. By only changing the inter-wire separation distance from 20 nm to 10 nm, keeping the other parameters the same, we see that about three more iterations are needed. This shows that for stronger interactions we need higher order correction terms of x. From eqs. (2.4) and (2.15) we see that the first iteration gives an x-term, the second iteration gives an x^2-term and so on.

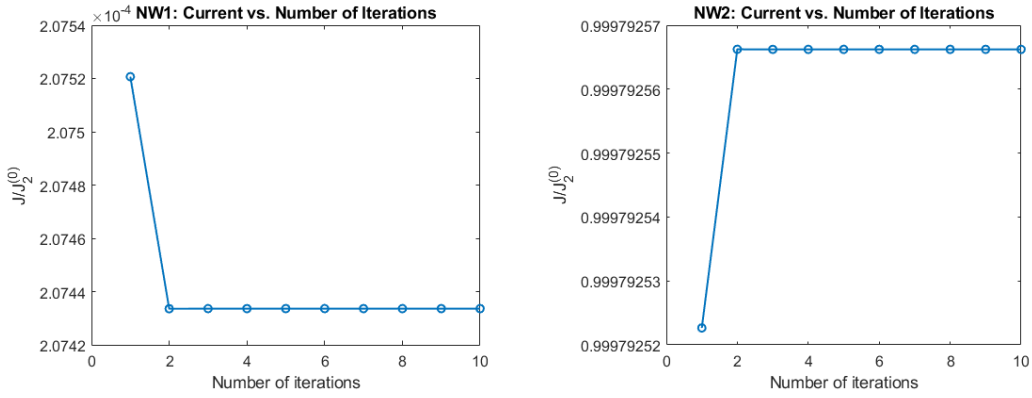

(A) (B)

FIGURE 3.4: Current in each wire as a function of number of iterations. The current has been normalized with the current of NW2 without interactions. In these results, the inter-wire separation distance is $d = 20$ nm.

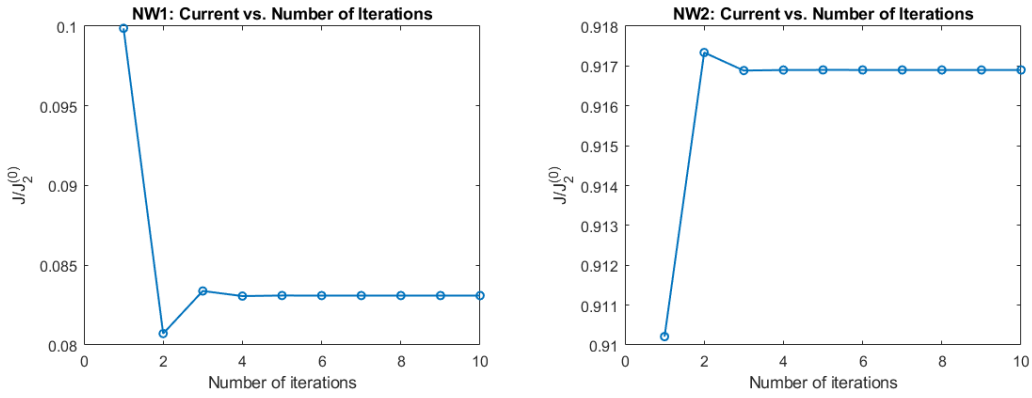

(A) (B)

FIGURE 3.5: Similar to figure 3.4 but with the inter-wire separation distance $d = 10$ nm instead.

3.3 Inter-wire distance dependence

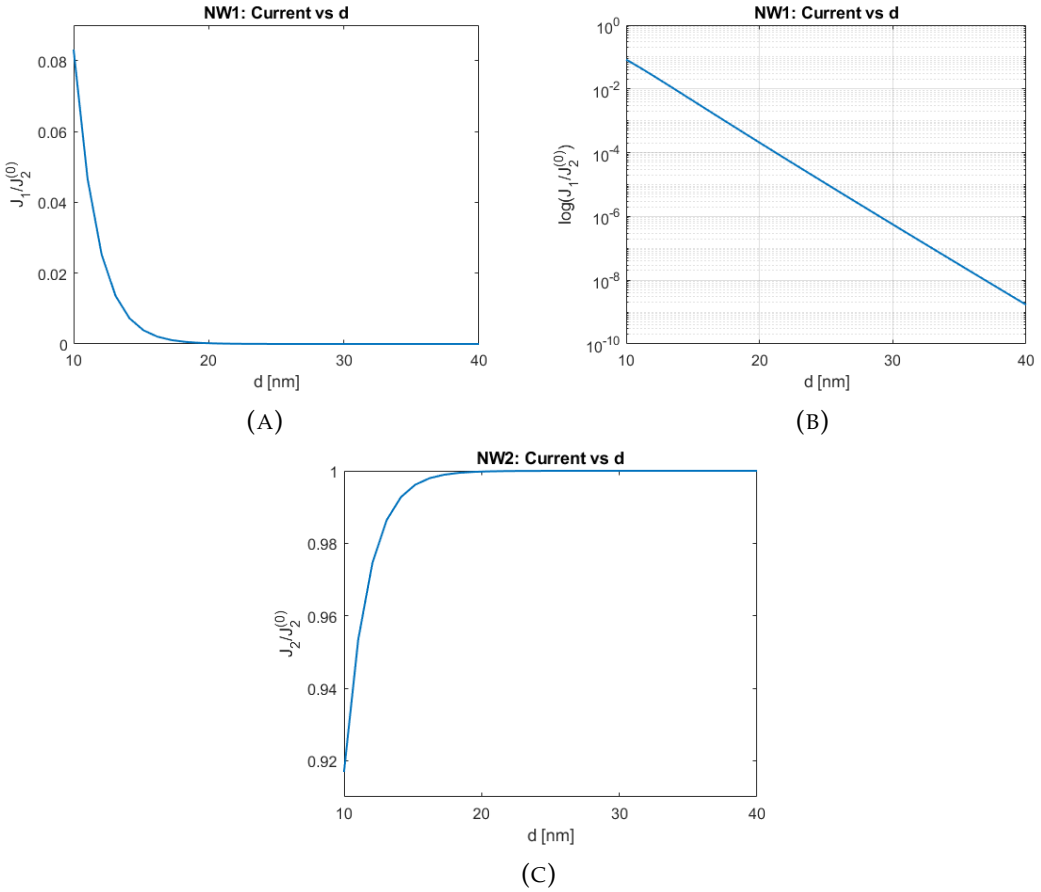

FIGURE 3.6: Inter-wire distance dependence. The current has been normalized by the current in NW2 without interactions.

Figure 3.6 shows how the current in each wire changes with respect to inter-wire separation distance. In NW1, we see that the current has an exponential dependence on the distance (see the semilogarithmic plot). Recall that in section 2.2, we showed that

$$K_0(\xi) = \sqrt{\pi/2}e^{-\xi}, \quad \xi \gg 1. \tag{3.1}$$

In our case $\xi = d|p_1 + p_2|/\hbar$, as seen from eq (2.23), and values of ξ in our implementation lies in the interval $0.6 < \xi < 5.5$. And since BTE's dependence of d only comes from K_0, we find that the current in NW1, in our case, exponentially decays as a function of d even when $\xi < 1$ does not hold.

The current in NW2 can be explained by the fact that the total current of our system remains constant, or equally the current gained in NW1 is the same amount of current lost in NW2. Without Coulomb drag there will only be a driving current in NW2, thus the total current of the system is always equal to the driving current before Coulomb drag takes effect, $J_2^{(0)}$. The fact that the total current remains unchanged is due to same effective mass in both wires and momentum conservation. Backscattering between electrons belonging to different wires results in a momentum transfer, where the momemtum lost in one electron is what the other gains. Since the magnitude of the momentum change is equal it can be shown that the magnitude of the current change is equal if the effective mass of both wires are equal.

Hence, the sum of the currents in both wires normalized by ($J_2^{(0)}$) should equal one, and this explains the shape of current in NW2 in figure 3.6C.

3.4 Bias Voltage dependence

The currents in NW1 and NW2 plotted as functions of bias voltage are presented here. The bias voltage is only changed across NW2, thus the voltage across NW1 remains zero. We show the bias voltage dependence of two cases, $eV \ll kT$ (small bias region) and $eV \geq kT$ (large bias region).

3.4.1 Small bias region

The temperature is $T = 1$ K, and the bias voltage varies from 1 to 20 μV. As seen in figure 3.7, both currents in NW1 and NW2 show a linear dependence. The linear dependence in NW1 agrees with the findings of Gurevich et al. [1]. The linear dependence in NW2 is also seen without the presence of Coulomb drag, see figure 3.8.

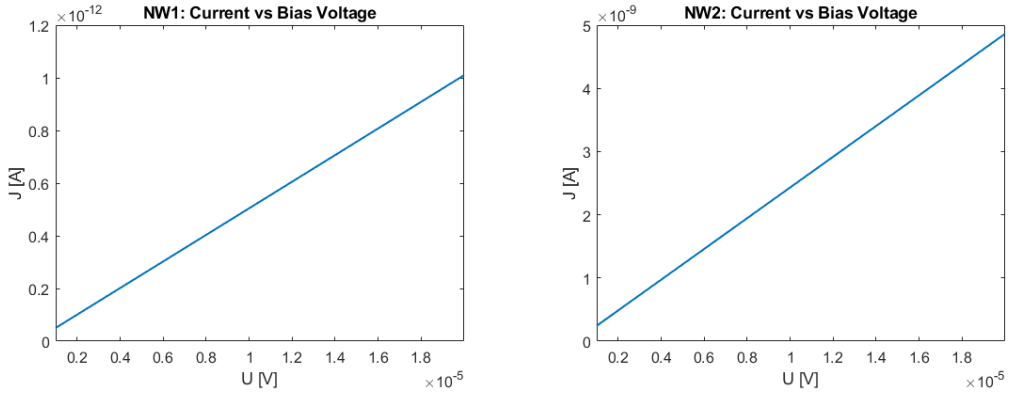

(A) (B)

FIGURE 3.7: The currents in (A) NW1 and (B) NW2 in the small bias region.

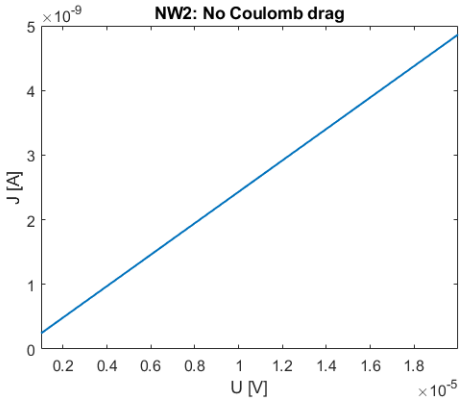

FIGURE 3.8: Current in NW2 without the presence of Coulomb drag.

3.4.2 Large bias region

The temperature is $T = 1$ K, and the bias voltage varies from 0.1 to 1 mV. Shown in figure 3.9 is the current in both wires in this range of bias voltage. We see that the voltage dependency in NW1 is no longer linear, and the current increases as the voltage increases. The current in NW2 still show a linear dependency as in the case of small bias. Since the current in NW1 has received a nonlinear contribution through Coulomb drag, the same must be true for the current in NW2. The reason that the current in NW2 still looks linear is because the magnitude of the nonlinear contribution is very small compared to the current in NW2 in the absence of Coulomb drag, which is linear (see figure 3.10).

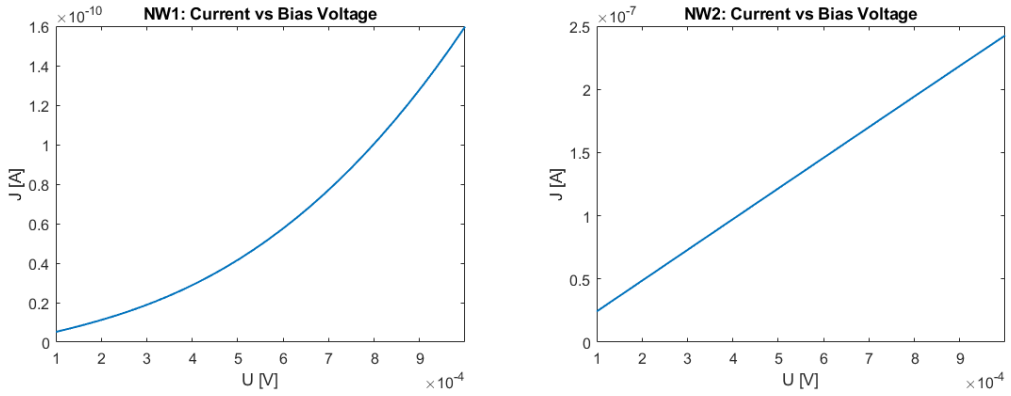

(A) (B)

FIGURE 3.9: Current in (A) NW1 and (B) NW2 in the large bias region.

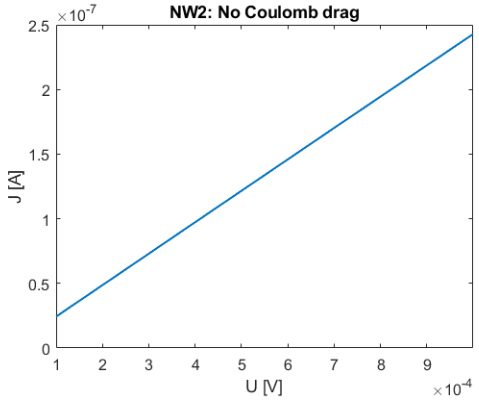

FIGURE 3.10: Current in NW2 without the presence of Coulomb drag.

3.5 Temperature dependence

Figure 3.11 shows the result of currents in NW1 and NW2 with varying temperatures with 0 V and $8.6\dot{1}0^{-6}$ V applied to NW1 to NW2, respectively. The range of temperature is 0.6 to 3 K. The temperature has been changed for both wires, meaning there is no temperature difference between both wires.

From the figure we see that the temperature dependence is almost linear in NW1. It makes sense that the current increases as temperature increases because the window of possible scatterings around the chemical potential is larger at increased temperatures. A wider range of p are available for scattering at higher temperatures because the distribution function is less steep around the chemical potential - there are more available states with p smaller than the Fermi momentum that electrons can scatter to and more electrons with p larger than the Fermi momentum can take part in the scatterings. As a result, the peak given by difference between the distribution functions of left and right moving electrons, see figure 3.3, would become wider.

In NW2, the shape of the current graph is not a result of Coulomb drag. Even without the presence of NW1 we find a similar shape of current with respect to temperature in NW2 in the presence of a bias voltage, see figure 3.12. There is no obvious difference between figure 3.11(B) and figure 3.12 which is due to the small bias ($V \ll 1$ K) applied on NW2 in the calculation, meaning the Coulomb drag is weak and the change in current in NW2 is small. The decline in current as T increases seen in figure 3.11 (B) and 3.12, is due to the reduced number of electrons in the conduction band which is a result of the chemical potential in our calculation has been fixed. In a real material, the chemical potential would not be fixed.

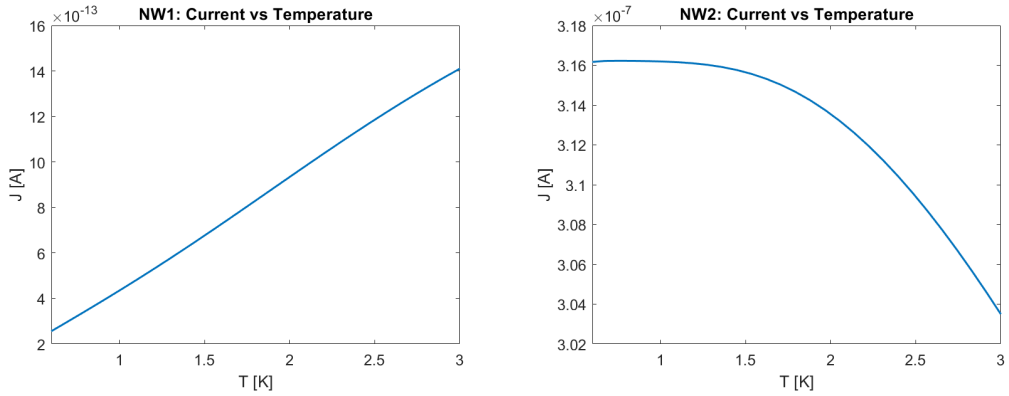

(A) (B)

FIGURE 3.11: Temperature dependence of current in (A) NW1 and (B) NW2.

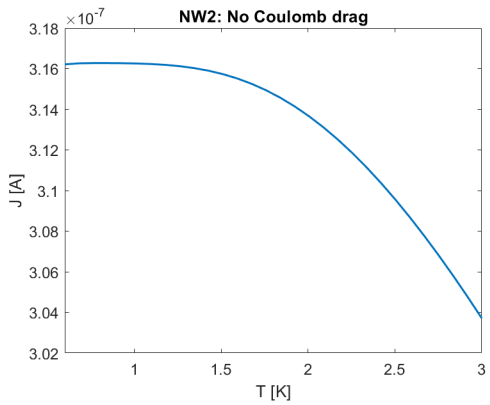

FIGURE 3.12: Current in NW2 without Coulomb drag.

Chapter 4

Conclusion

From our calculations, we have seen that the deviation, arising from Coulomb drag, in distribution functions from the equilibrium distributions are small when using the parameters we have used. The drag current has a exponential dependency of inter-wire separation distance in the passive wire. The currents in both the passive and active wires are linear in the small bias region which agrees with the results from Gurevich et al. [1], but nonlinear in the passive wire and (approximately) linear in the driving wire in the large bias region. Also, the drag current has almost a linear temperature dependence in the passive wire in our case and the temperature dependency is not dominated by the Coulomb drag between the wires. Lastly, the number of iterations required to reach a converged solution are few and parameters giving stronger interactions requires more iterations to reach convergence.

4.1 Outlook

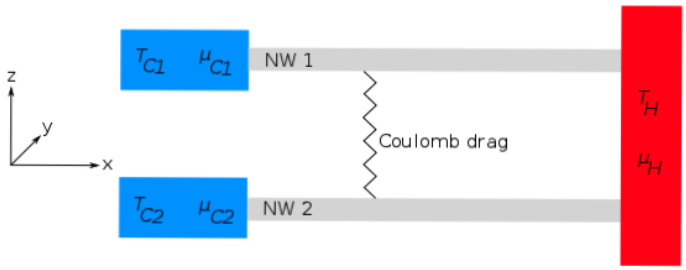

FIGURE 4.1: Model of a thermocouple comprised of two nanowires.

Our initial goal was to calculate the drag current in a thermocouple, see figure 4.1, although we did not manage to do this. The next step towards this goal would be to electrically connect the passive and driving wires as shown in figure 4.1, where one wire should be n-doped and another one p-doped similar to the TE device shown in figure 1.1. So far, the Coulomb drag has been introduced by an applied bias voltage on the driving wire. In a thermocouple, we would instead have a temperature gradient or difference along the wires to generate the Coulomb drag, where the temperatures are determined by the temperatures in the reservoirs.

But from the conclusion that the generated Coulomb current has the same direction as its driving current, the influence of Coulomb drag might decrease the performance of a thermocouple. As shown in figure 4.2, the current in the two wires are in opposite directions, which means the generated Coulomb current in each wire will be in opposite direction to the already existing current, unless having the wires

electrically connected and having a temperature gradient/difference can change this fact.

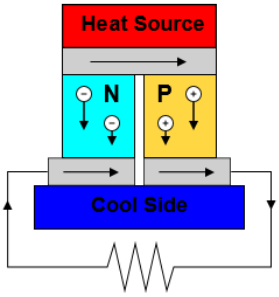

FIGURE 4.2: A thermocouple. Same figure as figure 1.1 in the introduction section.

Bibliography

[1]V. L. Gurevich, V. B. Pevzner, and E. W. Fenton, "Coulomb drag in the ballistic electron transport regime.", Journal of Physics: Condensed Matter **10**, 1 (1998).

[2]D. H.M. L. Günther Grossmann, Carina Fasth, *Fasta tillståndes fysik*.

[3]M. Lundstrom, "The boltzmann transport equation", in *Fundamentals of carrier transport*, 2nd ed. (Cambridge University Press, 2000), 119–157.

[4]B. Lon E., "Cooling, heating, generating power, and recovering waste heat with thermoelectric systems.", Science, 1457 (2008).

[5]B. N. Narozhny, and A. Levchenko, "Coulomb drag", Reviews of Modern Physics **88**, 025003, 025003 (2016).

[6]M. Shur, and L. Eastman, "Ballistic transport in semiconductor at low temperatures for low-power high-speed logic.", IEEE Transactions on Electron Devices **26**, 1677 (1979).

[7]J. H. Davies, *The physics of low-dimensional semiconductors : an introduction.* (Cambridge University Press, 1998).

[8]D. Laroche, "Coulomb drag in vertically-integrated one-dimensional quantum wires", PhD thesis (McGill Univeristy, 2014).

[9]R. Landauer, "Spatial variation of currents and fields due to localized scatterers in metallic conduction", IBM Journal of Research and Development **1**, 223–231 (1957).

[10]M. Büttiker, "Four-terminal phase-coherent conductance.", Physical Review Letters **57**, 1761–1764 (1986).

[11]M. B. Pogrebinksi, Fiz. Tekh. Poluprov. **11**, 372 (1977).

[12]A. P. Dmitriev, I. V. Gornyi, and D. G. Polyakov, "Coulomb drag between ballistic quantum wires.", (2012).

[13]K. Schonhammer, "Luttinger Liquids: The Basic Concepts", arXiv e-prints, cond-mat/0305035, cond–mat/0305035 (2003).

[14]P Debray, V. N. Zverev, V Gurevich, R Klesse, and R. S. Newrock, "Coulomb drag between ballistic one-dimensional electron systems", Semiconductor Science and Technology **17**, R21 (2002).

[15]P. Debray, V. Zverev, O. Raichev, R. Klesse, P. Vasilopoulos, and R. S. Newrock, "Experimental studies of coulomb drag between ballistic quantum wires.", Journal of Physics: Condensed Matter **13**, 1 (2001).

[16]M. Yamamoto, M. Stopa, Y. Tokura, Y. Hirayama, and S. Tarucha, "Negative coulomb drag in a one-dimensional wire.", Science, 204 (2006).